



OPEN Comprehensive analysis of temperature distribution in OPGW cable considering ramifications of short circuit current

Ahsan Ashfaq^{1,2✉}, Umair Khalique^{1,2}, Akif Nadeem³ & Arslan A. Rizvi³

Optical Ground Wire (OPGW) combines electrical conduction and telecommunication within overhead power transmission systems. This paper investigates the thermodynamics of OPGW after the occurrence of short circuits, with a primary focus on temperature increase and its implications for the optical fiber component after the occurrence of a short circuit that leads to a rise in temperature on the optical fiber. The key novelty of this study lies in the analysis of the after-effects of short circuits, particularly the heat dissipation over time and its impact on optical fiber attenuation, which has not been thoroughly addressed in previous studies. Our investigation addresses three cable configurations with distinct armor compositions having outer materials of steel and aluminum. The study is conducted using the finite element method that enables the investigation of the post short circuit effects by using the simultaneous computation of electromagnetic and thermodynamic equations, providing a comprehensive understanding of electrical and thermal effects. The study reveals that the cable with an outer aluminum and inner steel armor layer exhibits the lowest temperature rise of 62 °C at the optical fiber under a 15.4 kA short-circuit current, compared to 172 °C in outer steel armored design cable. This reduction is attributed to aluminum's lower permeability, which suppresses the skin effect. The aluminum-steel hybrid design also minimizes signal attenuation by 55% compared to the outer steel armored design cable.

Keywords Attenuation, Cable armor, Finite element method (FEM), Optical ground wire (OPGW), Thermal field distribution

In the rapidly evolving research in the twenty-first century, the demand for electricity in China has surged alongside the continuous development of society. To meet the increasing needs of this modern era, the construction of high-voltage power grids is accelerating. In this context, Optical Ground Wire (OPGW) has emerged as a central part having increasingly widespread application¹. As a cable with the unique dual functionality of serving as both a grounding element and a communication channel, OPGW boasts numerous advantages, including substantial communication capacity, robust resistance to electromagnetic interference, resilience against external damage, and cost-effective installation². The utilization of communication technology has permeated various aspects of the electric power system, with optical fiber communication, particularly OPGW (optical ground wires), being the preferred choice for newly built communication lines due to its performance in electrical and optical transmission^{3,4}. Yet, as OPGW cables traverse the vast expanse of the power grid, they are exposed to various potential damages, two of the most prevalent being atmospheric discharges and short circuits⁵. In instances of short circuits, high electrical currents surge through the OPGW structure, generating intense heating that can surpass the cable's maximum temperature tolerance. As such, understanding the thermal behavior of OPGW cables under short-circuit conditions becomes imperative, as it empowers the optimization of cable construction for specific applications^{6,7}. While previous studies have investigated the immediate effects of short-circuit currents on OPGW cables^{2,3}, there is a lack of research on the after-effects of short circuits, particularly the heat dissipation over time and its impact on optical fiber attenuation. This study addresses this gap by providing a comprehensive analysis of the thermodynamics of OPGW cables after short-circuiting events, focusing on temperature increase and its implications for the optical fiber component. The key scientific contributions of this work include the analysis of the heat dissipation process over time, providing insights into the long-term thermal

¹College of Intelligent Manufacturing and Digital Mining, Yuncheng Vocational and Technical University, Yuncheng 044000, China. ²Shanxi Hongyuan Group Co., Ltd, Linfen, Shanxi, China. ³School of Intelligent Manufacturing and Control Engineering, Qilu Institute of Technology, Jinan 250200, China. ✉email: ahsan.xjtu@gmail.com

behavior of OPGW cables after short-circuit events along with the explicit examination of the relationship between temperature increase and optical fiber attenuation, offering valuable insights for minimizing signal loss, and optimization of armor materials by comparing three cable configurations with distinct armor compositions (steel and aluminum), identifying the optimal design for minimizing temperature increase and enhancing thermal stability under short-circuit conditions. This paper embarks on an electro-thermal analysis, shedding light on the intricate thermodynamics of OPGW cables when subjected to short-circuit scenarios, to enhance their performance and reliability in the dynamic realm of power transmission.

As OPGW carries the function of grounding the power system, it is particularly susceptible to the effects of lightning strikes and short circuits in the power system⁸. To understand the complicated interaction between lightning-induced short circuits and the resulting thermal effects on OPGW, it is vital to investigate the dynamics of current distribution and the effect of heat dissipation in the cable after the occurrence of short circuit current along with the effect on the optical fiber. Traditionally, the temperature distribution in overhead line conductors has been analyzed under the assumption of uniform current distribution at the time of short circuit current flowing in the conductors, neglecting the influence of heat dissipation in the cable to develop the temperature equilibrium. Prior studies analyzed OPGW temperature distribution during short circuits using coupled FEM simulations but focused solely on steady-state and transient regimes (≤ 1 s)^{9,10}. While these works compared aluminum-steel armor configurations, they did not address post-fault thermal dissipation or its impact on optical fiber attenuation, which is a gap this study bridges. Recent work by L. Qu further highlights the criticality of material-specific thermal limits but lacks analysis of communication performance degradation under delayed heating¹¹. However, modeling the thermal behavior of OPGW cables during short-circuit events presents significant challenges, particularly due to the rapid temperature gradients that occur. These gradients change very quickly, making them difficult to capture accurately using the finite element method (FEM)^{12,13}. Previous studies have highlighted the limitations of FEM in simulating such rapid changes and have proposed alternative approaches, such as coupled electro-thermal simulations and inverse heat conduction problems (IHCP), to address these challenges¹⁴. In this study, we aim to mitigate these limitations by using non-adiabatic assumptions and combining the three different time studies in a single frame of simulation that first includes the normal current condition combined with the short circuit current condition and then is united with the after-effects of short circuits. This paper investigates the temperature field distribution of short-circuit events in OPGW, with a particular focus on the temperature increase and its effect on the optical fiber after the occurrence of short-circuit current. By considering different materials for conductors, we aim to provide a comprehensive understanding of the thermal challenges OPGW faces in short-circuit occurrences, advancing our knowledge in the quest for enhanced power grid resilience and reliability.

Many researchers have investigated the electro-thermal analysis of Optical Ground Wire (OPGW) cables, contributing valuable insights into the cable's behavior under various conditions. Z. Miro's work employed a mathematical framework based on Maxwell's equations and Bessel's functions to scrutinize the temperature distribution within OPGW, focusing on the significant influence of the skin effect¹⁵. However, it is noteworthy that this study did not account for the initial temperature conditions, suggesting potential areas for further exploration. L. Gonzalez conducted an extensive investigation into the thermal field distribution of OPGW cables during short-circuit events, incorporating variations in armor thickness and exploring the use of different materials⁹. Nevertheless, the study did not encompass an examination of the temperature dynamics experienced by the optical fiber component following short-circuit occurrences, highlighting an aspect that merits deeper exploration. In Victor's research study, the finite element method was employed to determine the optimal outer material for OPGW cables, with a specific focus on mitigating temperature spikes during short-circuit events¹⁰. While commendable, the study could potentially achieve a more comprehensive outlook by considering not only the temperature increase within the conductors but also the consequential thermal effects on the optical fiber component, thereby offering a more complete perspective on the cable's performance under stress. Jinru methodically examined the impact of lightning strikes on OPGW cables, employing high-precision damage measurement techniques^{16,17}. This study, although shedding light on lightning-induced damage, regrettably omitted an exploration of continuous current flow within OPGW and its potential implications on the attenuation of communication signals within the optical fiber. This represents an avenue for future research to explore. J. Lu ventured into the intricate dynamics of OPGW cable behavior during short-circuit conditions. Notably, this research considered both electromagnetic and thermal structural coupling using the finite element method, providing valuable insights into stress distribution among the conducting strands of OPGW cables¹⁸. K. Ivanov's exploration focused on the thermal sustainability and structural integrity of OPGW cables under the duress of short-circuit currents, predominantly induced by lightning strikes, thus contributing valuable insights into the cable's resilience¹⁹. Wei Pang conducted research aimed at determining the allowable duration for short-circuit currents to flow through OPGW cables, to enhance cable stability²⁰. Gang Liu assessed lightning-induced damage to OPGW cables, drawing comparisons between the effects of natural phenomena and the modeling of Joule heat and arc heat²¹.

While prior studies have investigated the immediate effects of short-circuit currents on OPGW cables, this work provides a novel comprehensive analysis of the delayed heat dissipation process and its impact on optical fiber attenuation, addressing critical gaps in existing research. Unlike previous approaches that focused solely on steady-state or transient regimes^{9,10}, our study combines three operational phases that are normal current flow, short-circuit event, and post-fault cooling phase in a unified finite element framework. This approach not only reveals how temperature continues to rise in optical fibers after fault clearance but also demonstrates the practical benefits of material optimization. Specifically, our results show that outer aluminum inner steel hybrid armor designs reduce post-fault temperature rise by 64% and attenuation by 55% compared to other configurations. These findings provide both theoretical advancements and practical solutions, establishing a new understanding of delayed thermal effects in OPGW and validated design criteria for improving grid

resilience and communication reliability. The coupled electro-thermal model developed here, which integrates electromagnetic and thermodynamic analysis while accounting for non-adiabatic conditions per IEC standards, represents a significant methodological improvement over prior adiabatic assumption. Finally, we have suggested that the cable with the outer armor layer of aluminum and inner armor layer of steel gives the advantage of a low temperature increase in the cable with a suppressed skin effect that results in lesser attenuation caused in the optical fiber after the occurrence of a short circuit.

Problem statement

The OPGW cable is intended to transfer both electricity and communication signals. The cable consists of multiple insulation layers; as the temperature at the conductor rises, heat transfers to the surrounding layers, causing the temperature at the optical unit to rise as well. In previous studies, the temperature increase on optical fiber is analyzed only at the time of occurrence of short circuit current; at that instance, the temperature increase at the optical fiber is negligible. The temperature increases in the optical fiber after the heat is dissipated due to the occurrence of a short circuit current. The increased temperature causes the insulation layers to expand, causing stress within the cable. The increase in temperature and stress is responsible for the increase in optical fiber attenuation. The attenuation increase due to the rise in temperature after a short circuit current is shown in Fig. 1.

The objective of this research is to comprehensively understand the thermodynamics of OPGW, specifically focusing on the temperature rise and its consequences for the optical fiber after short-circuiting events, prompting the exploration presented in this research with a specific emphasis on two distinct cable configurations that are steel and aluminum armor compositions. This study aims to address the gaps in knowledge and provide insights into enhancing OPGW resilience. The first problem is to use the finite element method and integrate the studies at different time periods to get the data for the temperature distribution after the occurrence of a short circuit current. The second problem is to compare the three different configurations of materials used for cable armor, which results in minimizing the temperature increase after the short circuit current passes through the cable, so the attenuation can be minimized.

OPGW cable configurations and specifications

In the study, three structures of OPGW cable are analyzed based on the materials used in the outer conductor layer. The most common structure of OPGW cable has either steel or aluminum in the outer conductors, which is shown in Fig. 2 named cable A, and two structures based on the modification made in the outer conductors are shown in Fig. 2. The modified structures are named cable B and cable C. In cable A, the outer conductor material is used as Aluminum. In cables B and C, aluminum, and steel combine to analyze the thermal field distribution after the short circuit current passes through the cable. The armor material combinations were selected based on IEC 60794-4-1²² and IEEE 1138²³ requirements for OPGW cables, which mandate both mechanical resilience and thermal stability during fault conditions. While commercial designs typically use homogeneous armor, either aluminum or steel, we propose hybrid configurations to address their respective limitations, all-aluminum designs lack sufficient strength for high-stress environments. In contrast, all-steel designs exhibit excessive heating due to pronounced skin effect⁹. Our Cable C places aluminum externally to optimize heat dissipation and current distribution, while the internal steel layer maintains structural integrity against mechanical loads.

In cable B, the inner cylindrical part of the outer conductor is aluminum (Material A), and the outer part is steel (Material B). In contrast, in cable C, the inner conductor is steel (Material B), and the outer part is aluminum (Material A). The outer radius of the cable is 8.73 mm, the radius of the inner conductors is 1.51 mm, and the thickness of the aluminum tube is 1.2 mm¹⁰. In the optical fiber unit, the material used for the heat-resistant layer is TPE, the material for the optical sheath is polyethylene PE, the optical fiber is immersed in

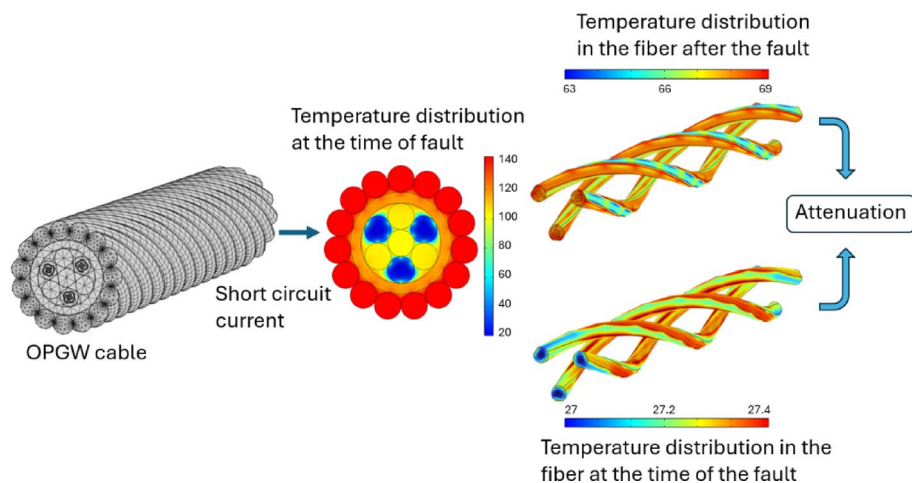


Fig. 1. The system diagram of the OPGW cable comprises temperature increase influencing the attenuation loss.

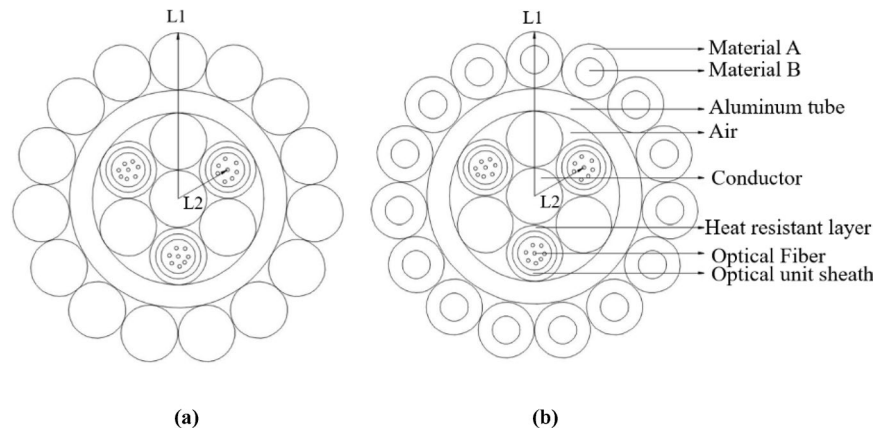


Fig. 2. The structure and materials of OPGW cable (a) OPGW cable A (armor is Aluminum), (b) OPGW cable B (outer armor is steel and inner is aluminum), and cable C (outer armor is aluminum and inner is steel).

Material	k [W/(m·K)]	ρ [kg/m ³]	σ [S/m]	C_p [J/(kg·K)]
Aluminum	211	2702	3.56×10^7	903
Fiber	0.144	871.0	1×10^{-15}	1850
Air	26.3e-3	1.161	1×10^{-15}	1.007
Aldrey	120	2703	3.05×10^7	909
Steel	40	6590	4.03×10^6	518

Table 1. Properties of materials.

polypropylene PP, and the optical fiber is made of silica glass. The cable's material characteristics encompass thermal conductivity (denoted as “ k ”), density (“ ρ ”), electrical conductivity (“ S/m ”), and specific heat capacity (“ C_p ”), as outlined in Table 1⁹.

The OPGW cables analyzed in this study are based on commercially available products manufactured by Shanghai Sun Telecommunication Co., Ltd. These cables adhere to IEEE 1138²³ and IEC 60794-4-1²² standards, ensuring high performance in electrical and mechanical properties.

Mathematical modeling

Mathematical modeling of temperature dependent attenuation

The optical signal attenuation in OPGW cables under temperature rise is governed by intrinsic absorption mechanisms, particularly OH ion vibrations. The total attenuation coefficient $\alpha(T)$ combines temperature-independent scattering losses and temperature-sensitive intrinsic absorption components given in Eq. (1)²⁴.

$$\alpha(T) = \alpha_R + \alpha_{UV} + \alpha_{IR} + \alpha_{OH} + \alpha_{IM} \quad (1)$$

Here, α_R is the attenuation loss by Rayleigh scattering, α_{UV} is the attenuation loss by ultraviolet absorption, α_{IR} is the attenuation loss by infrared absorption, α_{OH} is the attenuation loss by OH ions, and α_{IM} is the attenuation loss by impurities in optical fiber. The most prominent factor contributing to attenuation due to the increase in temperature is intrinsic absorption due to OH ions. The population distribution of OH ions follows quantum statistical mechanics, described by the Boltzmann factor given in Eq. (2).

$$N_v = \frac{N}{Q} \exp\left(-\frac{hcG(v)}{kT}\right) \quad (2)$$

Here, N is the total particle density, N_v is the population in the v^{th} vibrational state, Q is the partition function for vibrational states, h is Planck's constant, c is the speed of light, $G(v)$ is the vibrational spectrum term, k is Boltzmann's constant, T is the absolute temperature in Kelvins. The partition function Q encodes how temperature alters the accessibility of vibrational modes in the amorphous silica structure. Its logarithmic form derives from the Debye model with corrections for glassy materials given in Eq. (3).

$$Q = \beta \exp\left(\frac{\delta}{T} + \mu T^3\right) \quad (3)$$

Here, β , δ , and μ are material-specific constants that depend on the fiber composition and the vibrational characteristics of the material. The intensity of absorption, I_a , is proportional to the population of excited states and the transition probabilities, as governed by the molecular resonance absorption theory Eq. (4).

$$I_a = C_a v_0^2 \exp\left(-\frac{hcG(v)}{kT}\right) / Q \quad (4)$$

Here, C_a is a constant that combines the Einstein coefficient for spontaneous emission and the statistical weight of energy states, v_0 is the vibrational frequency associated with the ground state. The relationship between the intrinsic absorption loss and the attenuation coefficient is expressed as Eq. (5).

$$\alpha_i = -\frac{10}{L} \log\left(1 + C_1 T^3 \exp\left(-\frac{\delta}{T}\right)\right) \quad (5)$$

Here, L is the length of optical fiber cable, the dimensionless constant C_1 equals 0.0022 and the energy parameter δ is taken as 606 were determined via experimental fitting^{24,25}. The attenuation α_i increases with the temperature in a single-mode optical fiber used in OPGW is shown in Fig. 3.

Finite element model using coupled equations

The theoretical attenuation model reveals that temperature gradients drive the signal's power degradation. Building on the theoretical framework, we develop a coupled electro-thermal FEM model to simulate temperature distribution and attenuation dynamics in OPGW cables under short-circuit condition. The investigation of temperature distribution in OPGW cables during the flow of AC is conducted through modeling in COMSOL Multiphysics 6.3a²⁶. Unlike previous analyses that utilized ELEFANT 2D software for studying temperature distribution in OPLC cables, the current study in COMSOL incorporates a more comprehensive approach by considering heat transfer coupled with the magnetic field, allowing for a detailed examination of AC flow and temperature field distribution. To address the challenges of modeling rapid temperature gradients during short-circuit events, we employed a time-dependent study with sufficiently small time steps to capture transient thermal behavior. By IEC 60,826 and IEC 60,949, the non-adiabatic assumption was applied for conductor heating during a short circuit. This assumption accounts for heat dissipation to the surrounding environment, making it more representative of real-world conditions. The heat transfer coefficient for convection was set to 10 W/m²·K, as recommended by IEC 60,949 for natural convection in air. These standards informed our methodology for calculating temperature rise and evaluating the thermal stability of OPGW cables under short-circuit conditions. Specifically, the AC is induced to flow along the cable's axis within a magnetic field. The analysis employs Maxwell's equations in the frequency domain to derive solutions for the magnetic fields influencing the cable.

The density of the magnetic field (H), which results from the current density (J), is determined by Ampere's law, as expressed in Eq. (6). This governs the skin effect in OPGW armor layers, critical for modeling non-uniform current distribution during short circuits. The magnetic field solution, derived from Eq. (6), is used as input for the subsequent thermal analysis²⁵.

$$\nabla \times H = J \quad (6)$$

In the context of this analysis, where H represents the magnetic field density [A/m] and J stands for current density [A/m²], the connection between electric field intensity and current density is established by Maxwell's Ampere law. Utilizing this relationship, the study leverages COMSOL to generate the electric field within the conductor, thereby deriving the current density, as explained in Eq. (7)²⁷.

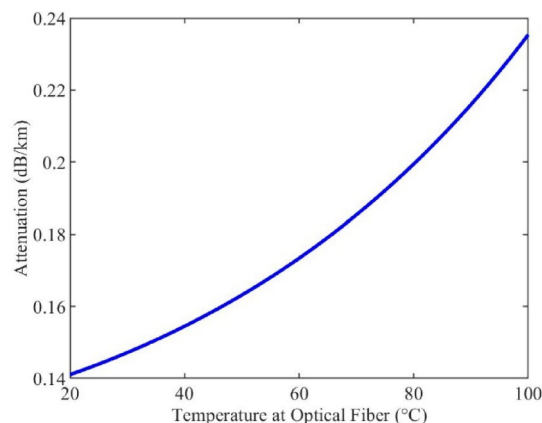


Fig. 3. Attenuation increases with the increase in temperature in optical fiber.

$$J = \sigma(E + v \times B) \quad (7)$$

The parameters involved include σ , representing electric conductivity; E , denoting electric field intensity; v , indicating the conductor's velocity; and B , representing magnetic flux density. This equation is solved in COMSOL's magnetic fields interface to compute the current distribution. The primary contributor to heat generation in the conductor is the resistive losses, denoted as Q_{rh} [W/m³], as illustrated in Eq. (8). The resistive heating term Q_{rh} bridges electromagnetic and thermal analyses.

$$Q_{rh} = \frac{|J|^2}{2\sigma} = \frac{\text{Re}(J \cdot E^*)}{2} \quad (8)$$

This term links electromagnetic simulations (1–2) to thermal analysis, where J is imported from COMSOL's frequency-domain solution. In the simulation process, the first law of thermodynamics is actively employed to quantify heat transfer within solids, accounting for resistive losses arising from electromagnetic waves. The magnitude of Q_{rh} depends on both the current density (J) and the material's electrical conductivity (σ), which focuses on the armor material selection, critically impacting temperature rise. The transient temperature field (T) is then governed by the heat transfer equation, which is the basis of the thermal analysis expressed in Eq. (9).

$$\rho C_P \frac{\partial T}{\partial t} = \nabla \cdot (k \nabla T) + Q_{rh} \quad (9)$$

Equation (9) represents the energy balance governing temperature evolution. The term $\rho C_P \cdot \partial T / \partial t$ accounts for thermal energy storage in the material. The term $\nabla \cdot (k \nabla T)$ models conductive heat transfer through Fourier's law, T is temperature [K] and k is the thermal conductivity [W/(m·K)]. The term (Q_{rh}) represents the volumetric heat source from resistive losses. According to Fourier's law of heat conduction, the rate of conductive heat flux is directly proportional to the temperature gradient as given in Eq. (10). This fundamental principle elucidates the relationship between the flow of heat within a material and the spatial temperature variation.

$$q = -k \frac{\partial T}{\partial x} \quad (10)$$

Here k is the thermal conductivity [W/(m·K)]. The time-dependent function is used to analyze the temperature distribution after the short circuit current flows in the cable by considering the transfer of heat.

Boundary conditions

The boundary conditions for the thermal analysis include heat transfer by convection from the cable surfaces to the surrounding environment. Radiation effects were considered negligible for this analysis due to the relatively low temperatures and the dominance of convective heat transfer in the ambient air environment. The heat transfer coefficient for convection was set to 10 [W/(m²·K)], a typical value for natural convection in air^{10,13}. The value for the convective heat transfer coefficient is calculated using the Churchill-Chu correlation for horizontal cylinders under natural convection. For a cable diameter of 8.73 mm the correlation is given by (11)²⁸.

$$h = \frac{k_{air}}{D} \left(0.60 + \frac{0.387 Ra^{1/6}}{[1 + (0.559 / Pr)^{9/16}]^{8/27}} \right)^2 \quad (11)$$

In this formulation, h represents the convective heat transfer coefficient [W/(m²·K)], k_{air} [W/(m·K)] is the thermal conductivity of air, Pr is the Prandtl number of air taken as 0.7²⁸, and D denotes the outer diameter of the OPGW cable. The dimensionless Rayleigh number Ra is calculated for characteristic conditions with gravitational acceleration. This correlation yields h equals to 9.7 [W/(m²·K)]. The calculated value of 9.7 [W/(m²·K)] is rounded to 10 [W/(m²·K)] to account for environmental variability while remaining within the IEC 60,949 range of 8–12 [W/(m²·K)]. This approximation is justified as our FEM results demonstrate minimal sensitivity to small variations in the heat transfer coefficient, with peak temperature differences of less than 1 °C observed during parametric testing. Furthermore, the selected value agrees with prior OPGW thermal studies^{9,10}. The cables were assumed to be located in an ambient air environment at a constant temperature of 27 °C. The short circuit current of 15.4 kA and frequency of 60 Hz is passed through the cable for 0.5 s, and two time-dependent studies are carried out together to analyze the after-effects of the short circuit current on the temperature increase in the cable, focusing on the optical fiber. The meshing of the OPGW cable is shown in Fig. 4.

The short-circuit current of 15.4 kA is selected based on industry standards IEC 60,949¹³ and IEEE 1138²³ for 220 kV transmission systems, where typical fault currents range from 10 to 20 kA. This value represents a practical worst-case scenario for OPGW cables, balancing realistic grid conditions with material thermal limits while enabling direct comparison with prior validated studies^{9,10} that used identical parameters.

Fe mesh independence

To ensure the accuracy of the FEM results, mesh independence tests were performed^{29–31}. The simulations were conducted using three different mesh sizes: coarse, fine, and extra fine shown in Table 2. The results for the temperature distribution and current density were compared across these mesh sizes to ensure convergence. The difference in results between the different mesh sizes was less than 2.2%, indicating that the fine mesh size

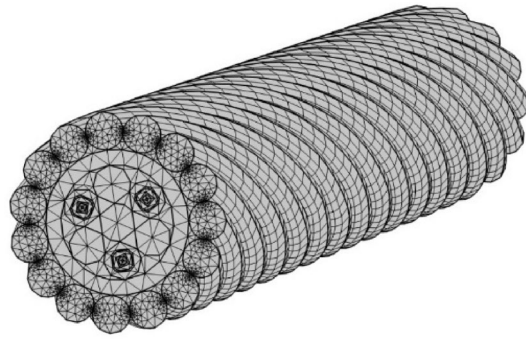


Fig. 4. The meshing of OPGW cable for applying FEM in COMSOL.

Mesh size	Elements	Maximum temperature [°C]	Error %
Coarse	11,376	145.1	2.2
Fine	25,296	142.0	Baseline
Extra fine	148,152	140.7	1

Table 2. Mesh sensitivity analysis of cable A.

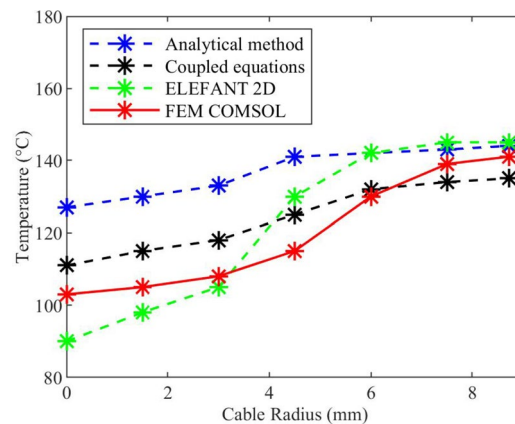


Fig. 5. Temperature distribution validation comparing our FEM results with previous results.

was sufficient for accurate simulations. Therefore, the fine mesh size was used for all subsequent simulations to balance computational efficiency and accuracy.

The model was validated against three established methods, including analytical solution using Maxwell's equations with Bessel functions, ELEFANT 2D simulations, and coupled electro-thermal equations¹⁰. As shown in Fig. 5, our results demonstrate <5% deviation in the conductor region while providing more accurate fiber core temperatures through improved treatment of interfacial thermal resistance.

The maximum temperature difference between fine and extra fine meshes was 1% (142.0 °C vs. 140.7 °C), confirming convergence as given in Table 2. The fine mesh was selected for all simulations to balance accuracy and computational efficiency. Numerical uncertainties were further minimized by employing the COMSOL MUMPS solver with a relative tolerance of 1×10^{-6} for coupled equations. Transient simulations used adaptive time-stepping with an initial step taken as 0.01 s, and a max. step taken as 0.01 s.

Simulation results

Analysis of temperature field distribution in cable A

In cable A, the outer armor is used as an Aldrey (Aluminum alloy) which is widely used in OPGW cable. The parameters of materials used in cable A are shown in Table I. In Fig. 6 (a) the temperature distribution along L1 is shown; the temperature variation is not very large as the material properties differ very slightly in aluminum and aldrety. The temperature in the center is comparatively lower than the temperature at the outer surface due to the skin effect.

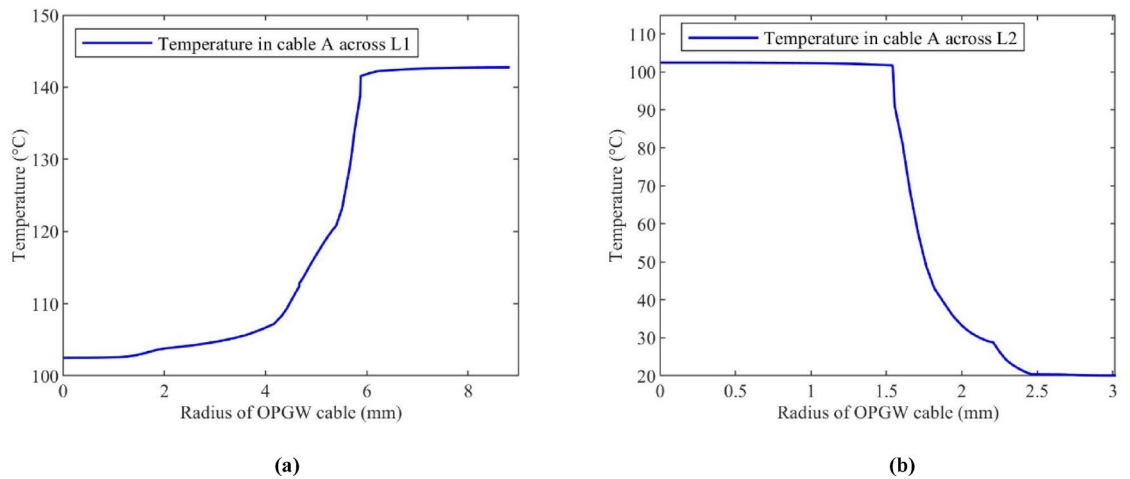


Fig. 6. The temperature distribution in cable A along (a) L1 and (b) L2.

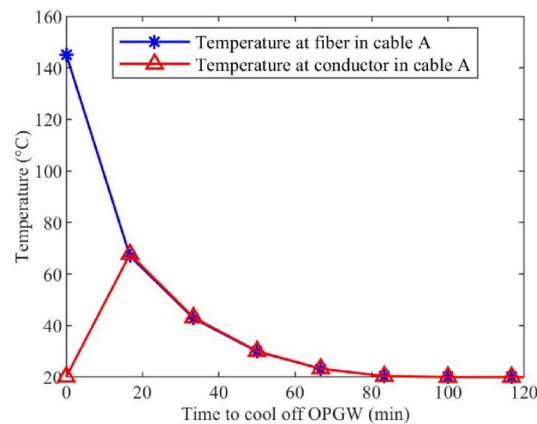


Fig. 7. The temperature field distribution is cooling off in cable A.

In Fig. 6 (b) the temperature distribution along the L2 is shown and it is seen that at the time of the short circuit current, the temperature at the optical fiber is negligible resulting in insignificant attenuation in the optical signal due to the difference of thermal conductivity of materials in the cable, the temperature at the optical fiber remains same as before the occurrence of fault. Further, by analyzing the simulated results, the heat transfers in the cable with time and the temperature at the fiber rises, increasing attenuation.

After the occurrence of a short circuit current, the heat is dissipated in the cable, and thermal equilibrium is attained with time, allowing the heat to transfer through optical fiber insulation layers. The temperature increase after the short circuit current is shown in Fig. 7. The temperature at the fiber first increases and then attains the thermal equilibrium to cool off with the cooling of the conductors. At the time of short circuit current, a very high current of 15.4 kA flows in the cable, which only increases the temperature of conductors in OPGW, but as time passes, the heat is dissipated, and slowly the temperature at the optical fiber increases up to 69 °C before cooling off. The simulation parameters, including the short-circuit current and time duration, were selected in accordance with IEC 60,826¹² and IEC 60,949¹³, which provide guidelines for evaluating the thermal behavior of overhead conductors under short-circuit conditions. This situation is simulated by combining time-dependent studies using FEM that allow to combine the different scenarios of short circuit fault flow and enables us to simulate the cooling off time after the flow of current in OPGW cable. This increase in temperature also affects the attenuation of the fiber. The temperature field distribution in the optical fiber unit is shown in Fig. 8.

Analysis of temperature field distribution in cable B

In cable B, the outer armor is steel, and the inner armor is aluminum. In this study, the ratio of inner and outer armor is taken as 0.5. In Fig. 9 (a), the temperature distribution along L1 is shown; the temperature in the cable is very high as the skin effect is prominent due to the outer layer of steel. The temperature in the center is also relatively high due to the prominent skin effect.

In Fig. 9 (b), the instance of the short circuit, it is seen that the temperature at the fiber is not changed and remains at the initial temperature, which causes negligible attenuation in the optical signal. However, after the

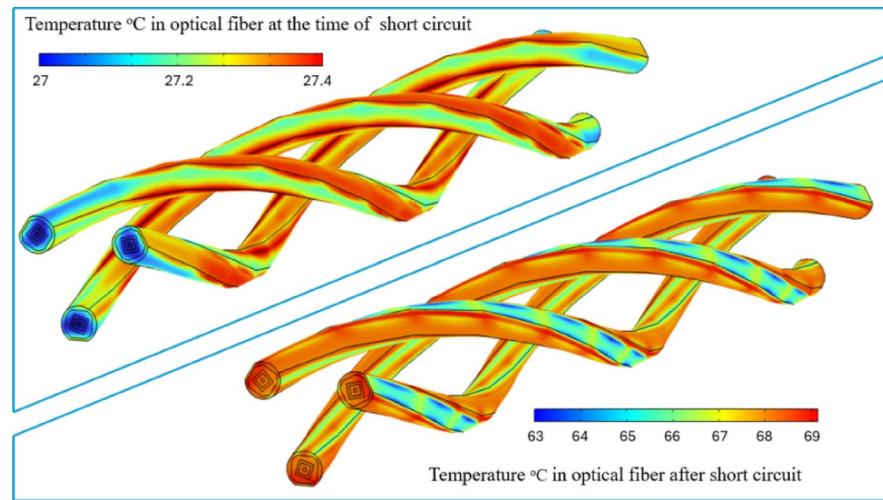


Fig. 8. The temperature field distribution at the optical fiber unit in cable A.

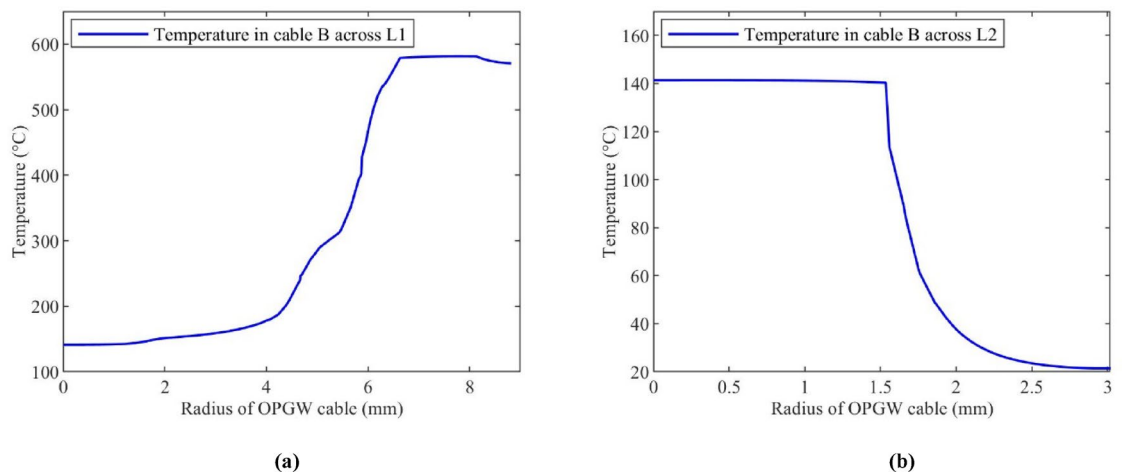


Fig. 9. The temperature distribution in cable B along (a) L1 and (b) L2.

short circuit, as the heat is dissipated around the cable materials, the temperature of the fiber rises before cooling down to the initial temperature shown in Fig. 10. This temperature rise is significant enough to cause attenuation in the optical fiber signal and can cause damage to the fiber.

Analysis of temperature field distribution in cable C

In cable C, the outer armor is Aluminum, and the inner armor is steel. In this study, the ratio of inner and outer armor is taken as 0.5. In Fig. 11 (a), the temperature distribution along L1 is shown; the temperature in the cable is slightly less than that of cable A as the outer armor is aluminum, which reduces the skin effect, so the current distribution is more uniform in the cable, and the temperature variation is less. Figure 11 (b) displays the temperature distribution along the L2. During the short circuit current, the temperature at the optical fiber is quite low, which causes the negligible attenuation in the optical signal.

Heat is dispersed throughout the cable following the occurrence of a short circuit current, allowing heat to pass through the insulating layers of optical fibers making the temperature rise at the optical fiber as 62 °C shown in Fig. 12.

Comparative analysis

The skin effect significantly amplifies the temperature rise in OPGW cables by concentrating current flow near conductor surfaces. As analyzed in^{9,10}, short-circuit currents (60 Hz) induce opposing eddy currents that force charge carriers toward outer layers. This effect is intensified in steel due to its high relative permeability $\mu_x \approx 280$ for mild steel^{9,23}, compared to aluminum, $\mu_x \approx 1$, which exhibits negligible magnetic properties. This creates non-uniform Joule heating, where current density J follows an exponential decay from the surface. In Cable B's steel-armored design¹⁰, 78% of current flows within the outer 0.5 mm, causing localized heating up to 570 °C versus 132 °C in aluminum-armored Cable C, where current distributes more uniformly.

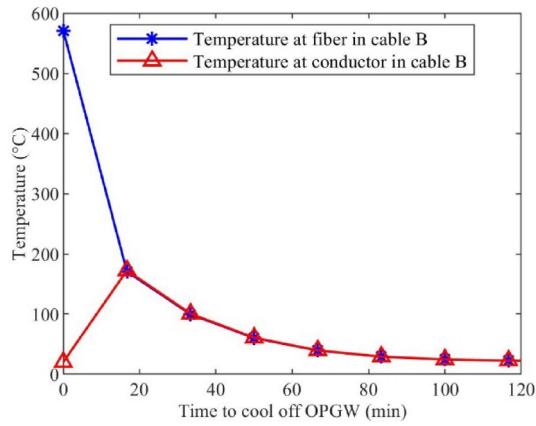


Fig. 10. The temperature field distribution is cooling off in cable B.

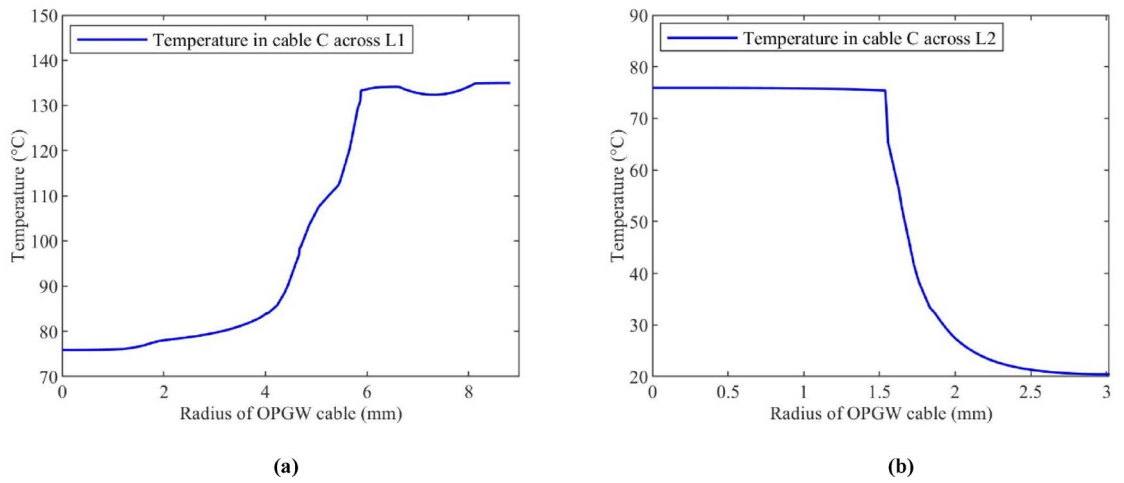


Fig. 11. The temperature distribution in cable C along (a) L1 and (b) L2.

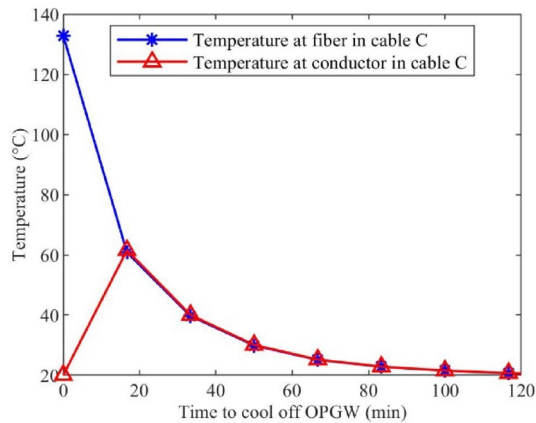


Fig. 12. The temperature field distribution is cooling off in cable C.

The comparison of the three cable designs reveals critical performance differences under identical short-circuit conditions. Cable C (Al/Steel) demonstrates superior thermal management, with a maximum conductor temperature of 132 °C that is 7% lower than Cable A (142 °C) and a remarkable 77% reduction compared to Cable B’s alarming 570 °C. This extreme temperature in Cable B (Steel/Al) approaches the melting point

of aluminum alloys, highlighting the risks of steel-dominated designs. The optical fiber temperatures follow a similar pattern, with Cable C maintaining the lowest peak at 62 °C compared to Cable B's 172 °C, directly attributable to aluminum's superior thermal conductivity. Comparative results using different parameters are shown in Table 3.

The cooling time differences reveal another critical design consideration. The quicker cooldown period of Cable C, suggests that aluminum's thermal diffusivity not only limits peak temperatures but also accelerates post-fault recovery. This has practical implications for grid resilience; faster cooling reduces cumulative thermal stress, potentially extending cable service life by years. Optical performance metrics further differentiate the designs, with Cable C maintaining attenuation at 0.165 dB/km during faults that is 9% lower than Cable A (0.18 dB/km) and 55% better than Cable B's 0.37 dB/km. These results demonstrate that while all-aluminum designs (Cable A) perform adequately, aluminum-steel hybrids (Cable C) offer superior thermal and optical stability.

Discussion

The primary focus of this research is to investigate the thermal field distribution in Optical Ground Wire (OPGW) cables under short-circuit conditions. The study considered two scenarios: one involving the conventional configuration with Aldrey as the armor material and another with modifications in the armor, incorporating two different materials that are combinations of aluminum and steel. The investigation extended beyond the typical single-layer armor configuration to explore the potential benefits of a two-layer cylindrical structure. Our results align with emerging trends in OPGW research. Recent work by Y. Chen¹ on 750 kV lines similarly identified delayed thermal effects but focused solely on aluminum armored cables. In contrast, our hybrid aluminum-steel design reduces peak temperatures, demonstrating material optimization's role in mitigating post-fault attenuation. Similarly, D. Guo⁶ highlighted lightning-induced short circuits but did not explore heat dissipation's impact on optical signals that is a gap our time-dependent FEM model address. These comparisons underscore that while recent studies advance fault modeling, our work uniquely bridges thermal dynamics and communication performance.

The comparative analysis provides critical insights for OPGW design optimization. Cable C's 77% lower conductor temperature (132 °C vs. 570 °C) compared to Cable B demonstrates the effectiveness of aluminum outer layers in mitigating fault-induced heating. This thermal advantage translates directly to optical performance, with Cable C's fiber temperature (62 °C) being 64% lower than Cable B's (172 °C), resulting in more stable signal transmission (0.165 dB/km vs. 0.37 dB/km). The 55% attenuation improvement in Cable C is particularly significant as it remains below the 0.2 dB/km threshold for high-speed communications, while Cable B exceeds this critical limit. The cooling characteristics offer additional design considerations. Cable C achieves 66-minute thermal recovery versus Cable B's 150 min, proving aluminum's capacity to simultaneously constrain maximum temperatures and improve post-fault cooling rates. This has practical implications for grid reliability, as faster cooling reduces cumulative thermal stress on both conducting and optical components. These findings indicate that while steel provides mechanical strength, placing aluminum in the outer layer (Cable C) optimizes the balance between structural integrity and thermal-optical performance, making it the preferred configuration for modern power grid applications.

The results presented here advance current understanding of OPGW thermal dynamics in several important ways. First, our time-dependent analysis captures the critical delay between short-circuit events and peak temperature effects on optical fibers, which is a temporal relationship that was absent in prior steady-state models¹⁰. As the previous work by Dmitriev⁹ and Gonzalez¹⁰ reported only instantaneous heating effects, we show how continued heat dissipation leads to significant temperature increases (up to 62 °C in Cable C) at the optical fiber unit after fault clearance. Second, the demonstrated 55% attenuation reduction in aluminum-steel hybrid designs provides quantitative evidence for material optimization strategies that balance electrical and thermal performance. This finding addresses a key gap in the work of Miro¹⁵ and Victor¹⁰, who analyzed material choices but did not correlate them with communication performance degradation. The combination of aluminum and steel in this manner aims to provide flexibility in cable production, catering to diverse applications. Understanding the thermal behavior of such configurations is vital for optimizing OPGW cable designs, especially under adverse conditions like short circuits. The study shows that the temperature increase at the optical fiber is significant after the occurrence of a short circuit current as the result of thermal equilibrium, compared to Dmitriev⁹, who reported peak temperatures only during short circuits, our time-dependent analysis reveals a delayed temperature rise that is 62 °C in Cable C due to post-fault heat dissipation. This phenomenon, absent from prior studies, directly correlates with optical attenuation. In cable B the temperature at the point of short circuit current is negligible but increases rapidly as the heat transfer occurs between the conductors and optical fiber before cooling down. The temperature rises to 172 °C, which results in higher attenuation. This higher temperature is due to the prominent skin effect of steel having lower electrical conductivity and higher resistance, which leads the current to flow more at the surface, resulting in a higher temperature being transferred

Parameter	Cable A (Al)	Cable B (Steel/Al)	Cable C (Al/Steel)
Max. Temp. at Conductor (°C)	142	570	132
Max. Temp. at Fiber (°C)	69	172	62
Time to cool off (min)	75	150	66
Max. attenuation (dB/km)	0.18	0.37	0.165

Table 3. Comparative analysis of cables.

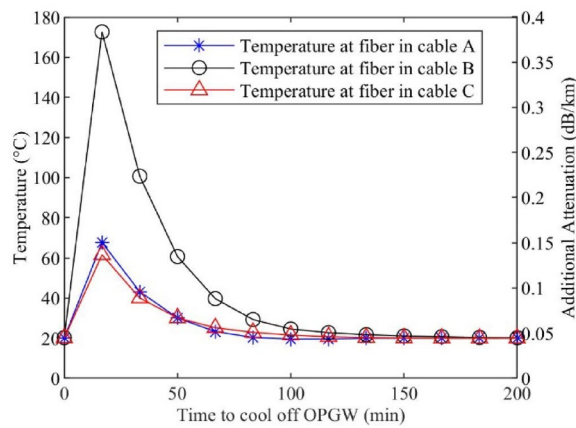


Fig. 13. Comparison of temperature and attenuation increase in OPGW cable configurations.

to the optical unit. In cable C, the outer layer is aluminum, allowing the reduction of the skin effect due to the combination of higher electrical conductivity and lower magnetic permeability that results in a lower increase in temperature at the optical fiber of 62 °C, resulting in lower attenuation^{24,27}. The comparison of temperature increase in the optical fiber after the occurrence of a short circuit is shown in Fig. 13.

The performance advantages demonstrated that the aluminum-steel hybrid design (Cable C) translates directly into actionable industry applications. Cable manufacturers can achieve the reduction in peak fiber temperature and lower attenuation by implementing an optimized design with an outer aluminum layer bonded to a high-strength steel core, maintaining compliance with IEC 60794-4-1 mechanical requirements. Power utilities should prioritize deploying such hybrid cables in transmission corridors with fault currents exceeding 10 kA or high lightning incidence, where the design's faster cooldown significantly reduces thermal stress on infrastructure. The consistent correlation between fiber temperature and attenuation further enables real-time monitoring, allowing operators to initiate cooling protocols when temperatures approach the 70 °C threshold that precedes signal degradation. This balanced approach, combining aluminum's thermal-electrical advantages with steel's structural resilience, offers a cost-effective upgrade path for existing grids while setting new performance benchmarks for future OPGW installations.

Conclusion

This study demonstrates that strategic material modifications in OPGW armor significantly improve thermal and mechanical performance under short-circuit conditions. The aluminum-steel hybrid design (Cable C) offers unparalleled advantages for OPGW cables under short-circuit conditions. Cable C achieves a peak optical fiber temperature of 62 °C, which is a 64% reduction compared to Cable B (170 °C), while maintaining signal attenuation at 0.165 dB/km, 55% lower than Cable B's 0.37 dB/km. The hybrid design enables 56% faster cooling, which is 66 min as compared to 150 min for Cable B, significantly reducing post-fault thermal stress. Mechanically, the inner steel layer enhances structural integrity, complying with IEC 60794-4-1 and IEEE 1138 standards for high-stress environments, while the outer aluminum layer optimizes current distribution and heat dissipation. This dual-material interaction ensures cable C surpasses conventional designs by maintaining attenuation below the critical 0.2 dB/km threshold. By integrating aluminum's thermal efficiency with steel's mechanical robustness, cable C establishes a benchmark for balancing grid resilience, communication reliability, and structural durability in modern power systems.

Data availability

The author confirms that all data generated or analysed during this study are included in this published article.

Received: 11 November 2024; Accepted: 26 June 2025

Published online: 01 July 2025

References

- Chen, Y. et al. Characteristic of power-transmission-induced current and power loss on the OPGW of 750 kv transmission line system. *Electr. Power Syst. Res.* **229**, 110130 (2024).
- Lecuna, R. et al. Non-contact temperature measurement method for dynamic rating of overhead power lines. *Electr. Power Syst. Res.* **185**, 106392 (2020).
- Sun, J. et al. Distributed transmission line ice-coating recognition system based on BOTDR temperature monitoring. *J. Lightwave Technol.* **39**, 3967–3973 (2021).
- Suhaimy, N., Radzi, N. A. M., Ahmad, W. S. H. M. W., Azmi, K. H. M. & Hannan, M. A. Current and future communication solutions for smart grids: A review. *IEEE Access.* **10**, 43639–43668 (2022).
- Chen, Y. et al. Analysis of induced voltage of optical fiber composite ground wire in 35 kv overhead distribution lines. *IEEE Trans. Electromagn. Compat.* **66**, 313–323 (2023).
- Guo, D. et al. An improved thermal damage evaluation method for lightning-induced failure analysis of overhead ground wire. *Eng. Fail. Anal.* **159**, 108095 (2024).

7. Guo, D., Liu, G., Chen, H., Wang, P. & Lin, X. Influence of structural characteristics for overhead ground wire on Arc root under lightning strike. *Electr. Eng.* **105**, 3283–3292 (2023).
8. Hu, K., Tong, F., Lian, W. & Li, W. Model and experimental verification of SOP transient in OPGW based on direct strike lightning. *Opt. Express.* **31**, 39102–39120 (2023).
9. Gonzalez, L. & Dmitriev, V. Electrothermal analysis of modified OPGW cables using multiphysics model. *Int Microw. Optoelectron. Conf* 1–5 (2015).
10. Dmitriev, V. & Gonzalez, L. Modified OPGW cable - Electrical and thermal analysis by coupled equations. *Int Microw. Optoelectron. Conf* 1–5 (2013).
11. Qu, L. et al. Study on thermal stability of OPGW in distribution line during lightning striking and grounding short circuit faults. *Int. Symp. Insul. Discharge Comput. Power Equip.* 673–682 (2023).
12. International Electrotechnical Commission (IEC). IEC 60826: Design Criteria of Overhead Transmission Lines. (2017).
13. International Electrotechnical Commission (IEC). IEC 60949: Calculation of thermally permissible short-circuit currents, taking into account non-adiabatic heating effects. (1988).
14. Xu, J. & Yuan, H. Analysis of temperature gradients in thin-walled structures under thermomechanical fatigue loading conditions. *Int. J. Fatigue.* **166**, 107254 (2023).
15. Zunec, M., Ticar, I. & Jakl, F. Determination of current and temperature distribution in overhead conductors by using electromagnetic-field analysis tools. *IEEE Trans. Power Deliv.* **21**, 1524–1529 (2006).
16. Sun, J. et al. Analytical investigation of lightning strike-induced damage of OPGWs based on a coupled arc-electrical-thermal simulation. *IEEE Trans. Power Deliv.* **37**, 5145–5155 (2022).
17. Sun, J., Yao, X., Huang, Y., Jiao, Z. & Chen, J. Experimental and numerical analysis of damage characteristics to OPGW strands under first lightning strike and continuous current. *Electr. Power Syst. Res.* **187**, 106515 (2020).
18. Lu, J., Liu, X., Shi, Z., Zeng, Y. & Luo, Y. Numerical analysis of terminal of armor rods for ground wire based on electromagnetic-thermal-structural coupling under the short-circuit current. *Int Conf. Power Energy Syst* 140–146 (2022).
19. Ivanov, K. & Uzunov, P. Coupled finite element analysis of optical ground wire for overhead power lines. *Int Conf. Energy Eff. Agric. Eng* 1–4 (2022).
20. Pang, W. & Zhang, Z. Study on measures to improve the short-circuit thermal stability of OPGW. *Conf Energy Internet Energy Syst. Integr* 1109–1113 (2022).
21. Jie, L., Gang, L. & Xi, C. Study on the thermal stability of OPGW under large current condition. *Pac -Asia Conf. Circuits Commun. Syst* 629–635 (2009).
22. International Electrotechnical Commission (IEC). IEC 60794-4: Optical fibre cables - Part 4: Aerial optical cables - Sectional specification. (2018).
23. Institute of Electrical and Electronics Engineers (IEEE). IEEE Std 1138: IEEE Standard for Testing and Performance for Optical Ground Wire (OPGW) for Use on Electric Utility Power Lines. (2019).
24. Yao, K., Chen, Y., Ashfaq, A., Sun, G. & Guo, Y. Power loss due to temperature rise in the optical unit of optical fiber composite low voltage cable. *Int Conf. Prop. Appl. Dielectr. Mater* 508–511 (2018).
25. Ashfaq, A. et al. Comprehensive analysis of temperature and stress distribution in optical fiber composite low voltage cable using finite element method. *IEEE Access.* **8**, 217380–217390 (2020).
26. COMSOL AB. *COMSOL Multiphysics* Version 6.3a. (2023). <https://www.comsol.com/>
27. Ashfaq, A. et al. Attenuation investigation influenced by the temperature and strain in an optical fiber composite low voltage cable. *Opt. Express.* **29**, 12696–12711 (2021).
28. Churchill, S. W. & Chu, H. H. S. Correlating equations for laminar and turbulent free convection from a horizontal cylinder. *Int. J. Heat. Mass. Transf.* **18**, 1049–1053 (1975).
29. Fadakar, F., Hosseini, S. M. H. & Merati Shirazi, A. H. Treeing modeling and the effect of rejuvenation fluid in aged XLPE power cables based on the finite element method. *Electr. Eng.* **106**, 7769–7781 (2024).
30. Liu, C. et al. Magnetic flux leakage, eddy current loss and temperature distribution for large scale winding in UHVDC converter transformer based on equivalent 2D axisymmetric model. *Electr. Eng.* **106**, 711–725 (2024).
31. Klimenta, D., Jevtić, M., Andriukaitis, D. & Mijailović, V. Increasing the transmission performance of a conventional 110 kv cable line by combining a hydronic concrete pavement system with photovoltaic floor tiles. *Electr. Eng.* **103**, 1401–1415 (2021).

Author contributions

[Author 1 Ahsan Ashfaq]: *Corresponding author, Conceptualization, Methodology, Writing, Simulation- original draft preparation. [Author 2 Umair Khaliq]: Data curation, analysis. [Author 3 Akif Nadeem]: Supervision, Writing - editing. [Author 4 Arslan A. Rizvi]: Supervision, Writing - review. All authors reviewed the manuscript.

Funding

Research funding is provided by Yuncheng Vocational and Technical University, Yuncheng, Shanxi, China. (No. KC20230103).

Declarations

Competing interests

The authors declare no competing interests.

Additional information

Correspondence and requests for materials should be addressed to A.A.

Reprints and permissions information is available at www.nature.com/reprints.

Publisher's note Springer Nature remains neutral with regard to jurisdictional claims in published maps and institutional affiliations.

Open Access This article is licensed under a Creative Commons Attribution-NonCommercial-NoDerivatives 4.0 International License, which permits any non-commercial use, sharing, distribution and reproduction in any medium or format, as long as you give appropriate credit to the original author(s) and the source, provide a link to the Creative Commons licence, and indicate if you modified the licensed material. You do not have permission under this licence to share adapted material derived from this article or parts of it. The images or other third party material in this article are included in the article's Creative Commons licence, unless indicated otherwise in a credit line to the material. If material is not included in the article's Creative Commons licence and your intended use is not permitted by statutory regulation or exceeds the permitted use, you will need to obtain permission directly from the copyright holder. To view a copy of this licence, visit <http://creativecommons.org/licenses/by-nc-nd/4.0/>.

© The Author(s) 2025